Stochastic synchronization via noise recycling

Marcello Borromeo[1,2] and Fabio Marchesoni[2,3,4]
[1]*Dipartimento di Fisica, Università di Perugia, I-06123 Perugia, Italy*
[2]*Istituto Nazionale di Fisica Nucleare, Sezione di Perugia, I-06123 Perugia, Italy*
[3]*Dipartimento di Fisica, Università di Camerino, I-62032 Camerino, Italy*
[4]*Michigan Center for Theoretical Physics, The University of Michigan, Ann Arbor, Michigan 48109-1120, USA*
(Received 18 January 2007; revised manuscript received 19 March 2007; published 12 April 2007)

The nonequilibrium escape dynamics in a bistable system under the influence of two Gaussian noises, one obtained by recycling, the other with a constant delay time, is shown by numerical simulation to exhibit stochastic synchronization; i.e., under stationary conditions, an appreciable fraction of renewal trajectories gets locked to the noise-recycling delay time. The conditions for optimal synchronization, reminiscent of stochastic resonance, are interpreted at any order within the framework of Kramers' theory.

DOI: 10.1103/PhysRevE.75.041106 PACS number(s): 05.40.−a, 04.80.Nn, 07.05.Dz

I. INTRODUCTION

Control or spurious signals, either periodic or noisy, while being transmitted across an extended system, may undergo time delays, due to diverse propagation mechanisms [1,2]. A good example is provided by the gravitational-wave interferometers, like the VIRGO detector [3]. Here, an external signal $\xi(t)$—e.g., a seismic disturbance—enters the antenna by creeping through its mechanical suspensions and eventually combines with the intrinsic noises in the apparatus, so that the detection signal $x(t)$, corresponding to the mirror displacement induced by the gravitational signal, is additively and multiplicatively affected by $\xi(t)$ at different times.

Noise delay can impact a variety of nonlinear phenomena, like the propagation of charge density waves [4], the migration of defects in crystalline materials [5], the transport of nanoparticles in biological [6] and artificial channels [7], the manipulation of vortex lines in superconducting devices [8], and colloidal particles along one-dimensional (1D) tracks [9]. However, its role has not been fully recognized yet, because in the current literature the multiple action of one noise source is often modeled by means of two or more *uncorrelated* noise terms. Delay effects have been studied in some detail only for the more controllable case of *periodic* input signals: A given phase lag between two additive signals [10] or between an additive and a multiplicative signal [11,12] may breach the spatial symmetry of the underlying x dynamics, thus inducing net currents [13] or asymmetric probability densities [14].

In this report we focus on the archetypal noise-activated process [15]

$$\dot{x} = ax - bx^3 + \zeta(t), \tag{1}$$

with modified stationary noise

$$\zeta(t) = \xi(t) + \epsilon\xi(t - \tau_d). \tag{2}$$

The stochastic variable $x(t)$ represents an overdamped Brownian particle confined to the double-well potential $V(x)=-ax^2/2+bx^4/4$; it overcomes the activation barrier $\Delta V=a^2/4b$ separating the two symmetric minima at $x_\pm = \pm\sqrt{a/b}$ thanks to the fluctuation source (2). Here, $\zeta(t)$ can be regarded as resulting from the linear superposition of a primary source $\xi(t)$ and a recycling term $\epsilon\xi(t-\tau_d)$, obtained by reinjecting a fraction $|\epsilon|$ of $\xi(t)$ after a processing time τ_d. Noise recycling should not be mistaken for a delay feedback, a mechanism also used to control activation processes [16].

The outline of this paper is as follows. In Sec. II the output of extensive numerical simulations is presented to illustrate how recycling delay affects the distributions of the particle escape times (to switch well) and of the renewal times (to escape and reenter the same well). Delay clocks renew events with duration τ_d, thus inducing an efficient mechanism of stochastic synchronization. Synchronization can occur at different orders, as the trajectories locked to the noise recycling procedure (2) can comprise multiple renewal cycles of different duration. In Sec. III the conditions for optimal synchronization at any order are analyzed within the framework of Kramers' activation rate theory. Practical applications of stochastic synchronization by noise recycling are briefly discussed in Sec. IV.

II. SIMULATION RESULTS

We characterized the noise-activated dynamics (1) and (2) by recording ordered sequences of the residence times $t_k^{(R)}, t_k^{(L)}, t_{k+1}^{(R)}, t_{k+1}^{(L)}, \ldots$: After having crossed the negative threshold $-x_{th}$, the particle takes a time $t_k^{(R)}$ to cross x_{th} and an additional time $t_k^{(L)}$ to recross $-x_{th}$, and so on, the index k counting the number of renewal, or recovery, cycles. The times $t_k^{(R)}$ and $t_k^{(L)}$ are two consecutive readings of the escape times $T_{R,L}$, respectively, to the right and to the left; the sum $\Sigma_{i=1}^{n}(t_{k+i}^{(R)}+t_{k+i}^{(L)})$ is the reading of the renewal time $T_r^{(n)}$ after n cycles. Due to the $x\to -x$ symmetry of $V(x)$, the mean escape times from one well into the other obey the identities $\langle T_{R,L}\rangle \equiv T_e = \langle T_r^{(1)}\rangle/2$. Moreover, for $D \ll \Delta V$ and $x_{th} \simeq |x_\pm|$, we can ignore the x_{th} dependence of the observables $T_{R,L}$ and $T_r^{(n)}$.

Without loss of generality we restrict our analysis to a linear combination (2) of zero-mean, Gaussian white noises with $0 \leqslant |\epsilon| \leqslant 1$, $\tau_d \geqslant 0$, and intensity D—i.e., $\langle \xi(t)\xi(0)\rangle = 2D\delta(t)$ and $\langle \zeta(t)\zeta(0)\rangle = 2D[(1+\epsilon^2)\delta(t)+\epsilon\delta(t-\tau_d)+\epsilon\delta(t+\tau_d)]$. Note that $x(t)$ defines an equilibrium process only for

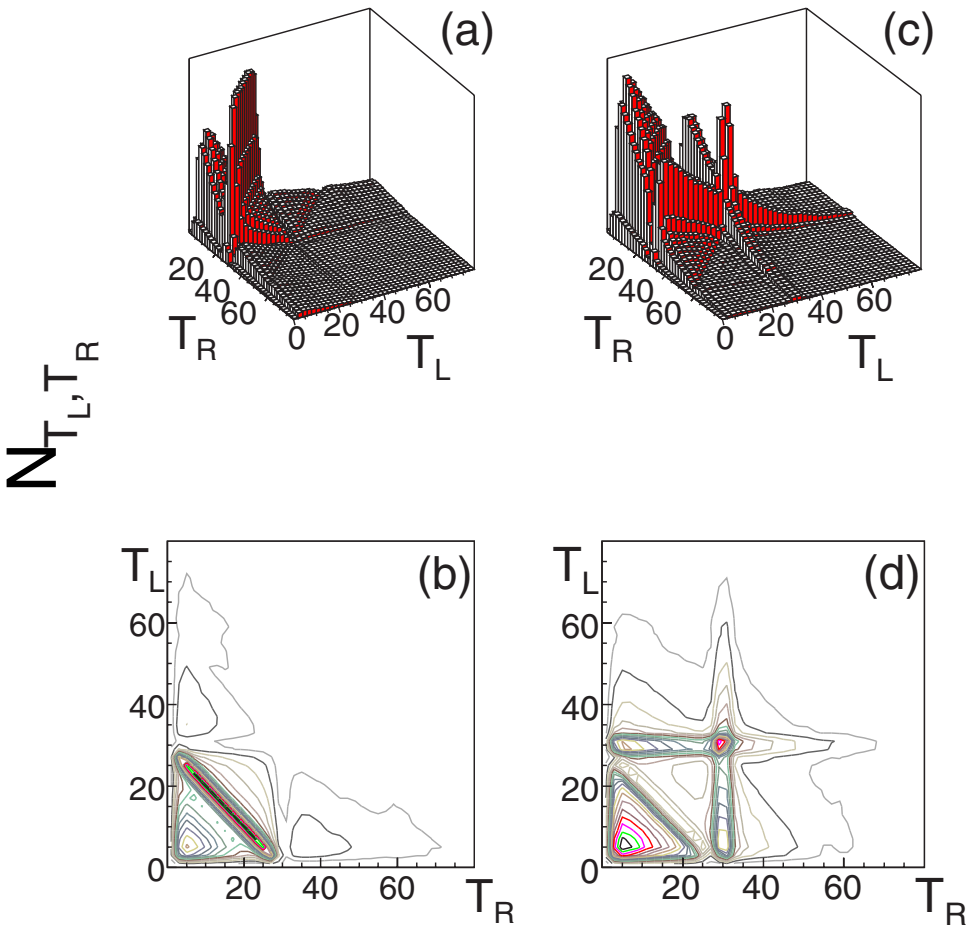

FIG. 1. (Color online) Statistics of the escape times of the process (1) and (2). Panels (a), (c) 3D plots of $N(T_R,T_L)$ for (a) $\epsilon=1$ and (c) $\epsilon=-1$; panels (b), (d) the corresponding contour plots for (b) $\epsilon=1$ and (d) $\epsilon=-1$. Other simulation parameters: $a=b=1$, $\Delta V/D=3$, $x_{th}=1$, and $\tau_d=30$.

$\tau_d=0,\infty$, when $\zeta(t)$ has intensity $D_0=2D(1+\epsilon)^2$ and $D_\infty=D(1+\epsilon^2)$, respectively.

The probability densities of the residence time pairs $t_k^{(R)}, t_k^{(L)}$, $N(T_R,T_L)$, are displayed in Fig. 1 for $\epsilon=1$ [panels (a) and (b)] and $\epsilon=-1$ [panels (c) and (d)]. For $\tau_d>0$, both the 3D [panels (a) and (c)] and the contour plots [panels (b) and (d)] exhibit a richer landscape than in the equilibrium case [15]. A sharp structure crosses the plane (T_R,T_L) along the diagonal

$$T_r^{(1)}=T_R+T_L=\tau_d, \tag{3}$$

forming a ridge (rift) depending on the sign of ϵ. This is the most prominent signature of stochastic synchronization induced by noise recycling (2) with $\epsilon>0$ ($\epsilon<0$). Also noticeable is the marked depression (peak) centered at the intersection of the secondary valleys (ridges) along the vertical and horizontal lines $T_{L,R}=\tau_d$, respectively. Finer structures at higher τ_d are hardly detectable with the present statistical accuracy.

To resolve more details, in Figs. 2(a) and 2(b) we plot the corresponding probability densities of the escape times $T_{R,L}$ and $N_{R,L}(T)$ and the renewal times $T_r^{(1)}$ and $N_r^{(1)}(T)$, respectively, for $\epsilon=\pm1$. These curves can be obtained by suitably integrating the relevant $N(T_R,T_L)$ plots with $\epsilon=1$ ($\epsilon=-1$). In correspondence with the main ridge (rift) of $N(T_R,T_L)$, the curves $N_{R,L}(T)$ develop an initial branch that appears to decay faster (slower) than their tail [17]; the perpendicular valleys (ridges) of $N(T_R,T_L)$ with $T_{R,L}=\tau_d$ are reflected by the $N_{R,L}$ dips (peaks) at τ_d. The pronounced synchronization peak (dip) of the curves $N_r^{(1)}(T)$ at τ_d coincides, instead, right with the diagonal structure of $N(T_R,T_L)$. Moreover, all peaks in $N_r^{(1)}(T)$ are mirrored by dips in $N_{R,L}(T)$ and vice versa, no

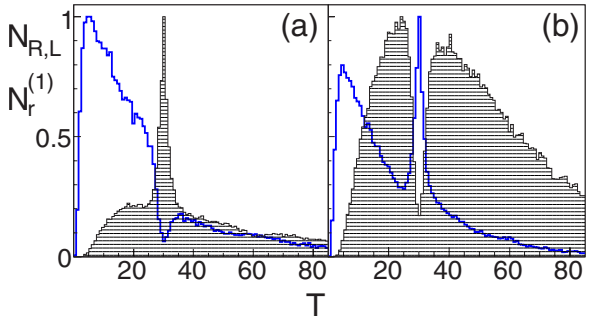

FIG. 2. (Color online) Statistics of the escape and the renewal times of the process (1) and (2): probability densities $N_{R,L}$ (blue solid curve) and $N_r^{(1)}$ (shaded) corresponding to the plots of Fig. 1.

matter what the sign of ϵ. Finally, we notice that the small dip [peak] of $N_r^{(1)}(T)$ [$N_{R,L}(T)$] at $2\tau_d$ is independent of the ϵ sign.

A simple interpretation of the synchronization phenomenon illustrated in Fig. 1 can be formulated more effectively in terms of renewal times than of escape times [18]. Let the Brownian particle execute two switches—say, left to right and back—within the time interval τ_d; the probability that it can retrace the same (or a close) trajectory over a subsequent time interval of the same length depends on the sign and the intensity $\epsilon^2 D$ of the recycled $\zeta(t)$ component; that is, the renewal events are not statistically independent [21]. For $\epsilon=1$ repeated renewal trajectories of duration τ_d are favored, as long as the individual escape times obey the synchronization condition (3). For $\epsilon=-1$ the sign of the recycled noise sequence acting on the particle after a renewal cycle of duration τ_d is opposite to the sign of the primary noise during the renewal cycle just completed; the particle is thus prevented from retracing the same escape path and recovery after τ_d gets unlikely. In other words, noise recycling (2) causes a spontaneous symmetry breaking of the dynamics (1).

The argument above explains, for instance, the existence of the diagonal ridge (3) of $N(T_R,T_L)$ for $\epsilon=1$ [Figs. 1(a) and 1(b)] and of the corresponding peak of $N_r^{(1)}(T)$ at τ_d [Fig. 2(a)]. By the same token we also understand why in Fig. 2 the curve $N_{R,L}(T)$ develops a dip in coincidence with a peak of $N_r^{(1)}(T)$ and vice versa. Suppose that under the action of a primary noise sequence of duration τ_d the particle has simply switched well; as the same $\xi(t)$ sequence is now recycled and fed into the system, the particle finds itself in a well with opposite symmetry with respect to the initial one: For $\epsilon>0$ it is unlikely that it can follow its path backwards (hence the $N_{R,L}$ dip), whereas dynamically equivalent initial conditions are restored by changing the sign of ϵ (i.e., $N_{R,L}$ peaks at τ_d for $\epsilon<0$). All remaining distribution peaks and dips shown in Figs. 1 and 3 are actually explained by this simple argument.

Our renewal time analysis is further corroborated by Fig. 3, where only the case $\epsilon=1$ is shown. In panel (a), $N_r^{(1)}(T)$ is plotted for increasing τ_d. While peaks and dips (the latter ones not always discernible) have been already identified as synchronization effects, the broad $N_r^{(1)}$ backgrounds represent the dominant fraction of independent renewal events. Such backgrounds are well fitted (not shown) by the Erlang functions $(T/T_e^2)e^{-T/T_e}$, where T_e depends on τ_d. According to the renewal theory [21], this fitting law becomes exact for $\tau_d=0$ and ∞, where T_e coincides with the Kramers' rates [18] $T_k(4D)$ and $T_k(2D)$, respectively (dashed curves). The synchronization peak amplitude, a resonant function of τ_d, reaches its maximum as the peak moves past the tip of the underlying $N_r^{(1)}$ background; no synchronization peak is visible for $a\tau_d \lesssim 3$ [Fig. 3(a), inset].

The probability densities of $T_r^{(n)}$ displayed in Fig. 3(b) for $\epsilon=1$, exhibit n peaks of decreasing amplitude at $T_r^{(n)}=m\tau_d$, with $m=1,2,\ldots,n$ (a few hardly detectable as they merge in the background). This means that feeding a recycled noise sequence of duration τ_d with $\epsilon>0$ into the system favors trajectories executing any integer number n of full recovery

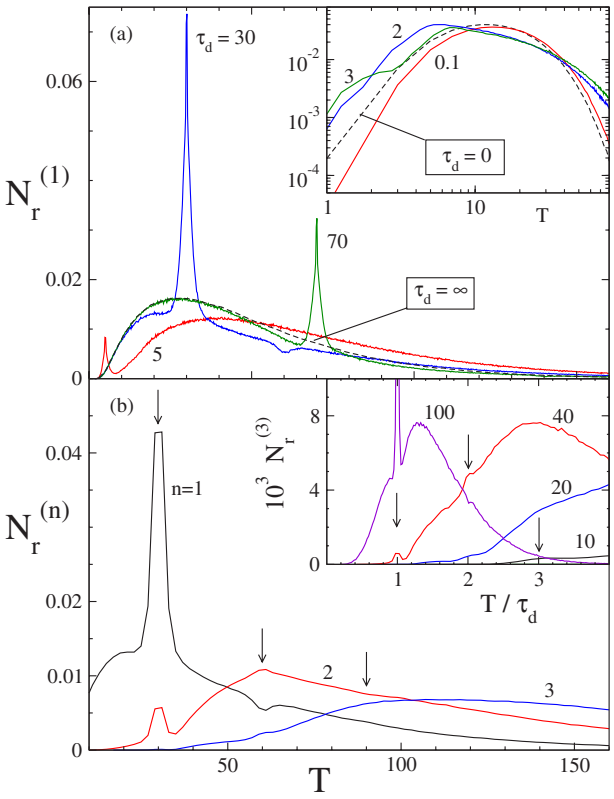

FIG. 3. (Color online) $N_r^{(n)}(T)$ for $\epsilon=1$ and different τ_d: (a) dependence of the $N_r^{(1)}$ synchronization peak on τ_d and (b) synchronization peaks for $n>1$. Vertical arrows indicate the renewal times $m\tau_d$ with $1\leq m\leq n$ (see text). Other simulation parameters: $a=b=1$, $\Delta V/D=3$, and $x_{th}=1$.

cycles in the time τ_d. Furthermore, we checked that only $N_r^{(1)}(T)$ develops a discernible dip at $2\tau_d$; high-m peaks can be made more visible by tuning D or τ_d (see inset); the width of the $N_r^{(n)}$ peaks is insensitive to n and m; the $N_r^{(n)}$ background, instead, broadens with increasing n, being well reproduced by the Erlang function $(T^{2n-1}/T_e^{2n})e^{-T/T_e}$.

The first peak of $N_r^{(n)}(T)$ with $m=1$, is the most prominent; the single renewal cycles contributing to the primary $N_r^{(n)}$ peak may still have different duration, so that no $N_r^{(1)}$ peak at τ_d/n is to be seen. The secondary peaks with $m>1$ are also revealing: as $N_r^{(1)}(T)$ peaks at $T_r^{(1)}=\tau_d$, the last peak of $N_r^{(n)}(T)$, $m=n$, measures the frequency of the sequences of n consecutive renewal cycles, each of duration τ_d; the second to last peak $m=n-1$ accounts for all consecutive combinations of $n-1$ renewal cycles of duration τ_d plus one double renewal cycle of duration $T_r^{(2)}=\tau_d$ [see first peak of $N_r^{(2)}(T)$], and so on, counting all possible combinations. Clearly, the higher m, the more conditional are the synchronized renewal trajectories of a given order n and the weaker their signature.

III. DISCUSSION

A quantitative analysis of the synchronization mechanism is sketched in Fig. 4, where the mean escape time T_e and the peak strength P_1 of $N_r^{(1)}(T)$ are plotted versus τ_d for $\epsilon=\pm 1$.

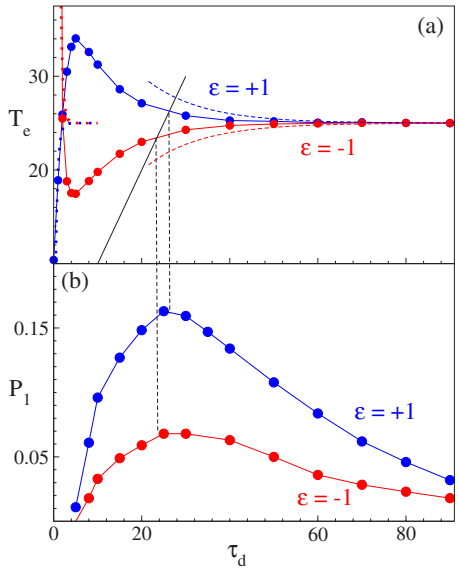

FIG. 4. (Color online) Resonance mechanisms for $\epsilon=\pm 1$: (a) T_e vs τ_d. Short and long τ_d approximations (see text) are represented by dotted and dashed curves, respectively. The intersection of each data set with the solid line $T_e=\tau_d$ defines the optimal synchronization condition in (b). (b) Peak strength of $N_r^{(1)}(T)$, P_1, vs τ_d.

P_1 is defined here as the area enclosed by the $N_r^{(1)}$ peak or dip at τ_d, taken with respect to the background of the uncorrelated renewal events. Two distinct resonant mechanisms, both induced by noise recycling, become apparent: $T_e(\tau_d)$ in Fig. 4(a) reaches a maximum ($\epsilon=1$) or a minimum ($\epsilon=-1$) for $a\tau_d \simeq \pi$; P_1 in Fig. 4(b) peaks for $\tau_d^{(P)} \simeq T_k(2D)$, regardless of the ϵ sign. The resonant behavior of $T_e(\tau_d)$ is controlled by the intrawell relaxation in the presence of noise recycling [19], whereas optimal synchronization—i.e., the P_1 maximum—results from the matching of delay and activation time scales.

For *short* delay times $a\tau_d \ll 1$, stationarity is set inside either potential well way before the escape process gets activated; $T_e(\tau_d)$ can be then written as an equilibrium Kramers' time [1] $T_e(\tau_d)=(2\pi/\omega_\pm\omega_0)[1+(3/8)(D_\tau/\Delta V)+\cdots]e^{\Delta V/D_\tau}$, where $\omega_\pm^2=V''(x_\pm)=2a$, $\omega_0^2=|V''(0)|=a$, and D_τ is an *ad hoc* function of τ_d. For $D \ll \Delta V$, the Brownian dynamics (1) and (2) inside a single well can be linearized as [13]

$$\dot{x} = -\omega_\pm^2(x \mp x_\pm) + \zeta(t). \tag{4}$$

This is a Gaussian process with steady-state variance $\sigma^2=D_\tau/\omega_\pm^2$ and $D_\tau(\tau_d)=D[(1+\epsilon^2)+2\epsilon e^{-\omega_\pm^2\tau_d}]$. The corresponding Kramers-like expressions for $T_e(\tau_d)$, plotted in Fig. 4(a) (dotted curves), bridge monotonically the exact equilibrium values $T_e(0)=T_k(D_0)$ and $T_e(\infty)=T_k(D_\infty)$ on the intrawell time scale $2\pi/\omega_\pm^2$.

For *long* delay times $\tau_d \gtrsim T_e(\tau_d)$, noise recycling modulates in time the interwell dynamics; indeed, synchronization peaks were observed only for $a\tau_d > \pi$ [Fig. 3(a), inset]. The interwell relaxation obeys asymptotically the linearized Langevin equation (1)

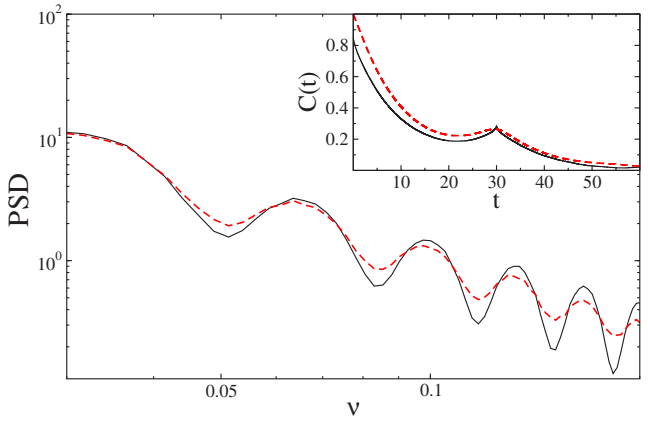

FIG. 5. (Color online) Autocorrelation effects induced by delay: PSD (main panel) and ACF (inset) of $x(t)$ for $\epsilon=1$ and $\tau_d=30$ prior to (black) and after filtering (red). Other simulation parameters are as in Fig. 1.

$$\dot{x} = -\mu x + \zeta_1(t), \tag{5}$$

where $\mu=2/T_k(D_\infty)$ and $\zeta_1(t)=(\omega_\pm^2/\mu)^{1/2}\zeta(t)$. The ensuing stationary autocorrelation function (ACF) of the process, $\langle x(t)x(0)\rangle=[1+(\epsilon/2)e^{-\mu\tau_d}]C_\infty(t)+(\epsilon/2)C_\infty(t-\tau_d)$, with $C_\infty(t)=(2D/\omega_\pm^2)e^{-\mu|t|}$, corresponds to the relaxation time

$$T_e(\tau_d) = (1+\epsilon e^{-2\tau_d/T_k(2D)})T_k(2D), \tag{6}$$

also plotted in Fig. 4(a) (dashed curves). In conclusion, the resonant behavior of $T_e(\tau_d)$ is due to the competition of intrawell and interwell dynamics.

The resonant curves $P_1(\tau_d)$ in Fig. 4(b) have a much simpler explanation. Synchronization by noise recycling operates by locking the process to trajectories that happen to complete n full renewal cycles within the delay time τ_d. Of course, the higher the density of such trajectories, the stronger the synchronization effect; for instance, for $n=1$, $P_1(\tau_d) \propto N_r^{(1)}(\tau_d)$. Moreover, we already know that the $N_r^{(n)}$ background is an Erlang function of order $2n-1$ with maximum at $(2n-1)T_e(\tau_d)$; hence, the optimal synchronization condition $\tau_d^{(P)}=T_e(\tau_d^{(P)})$ for $n=1$. This equation, solved graphically in Fig. 4(a), as the intersection point of our numerical data sets with the line $T_2=\tau_d$, closely locates the position $\tau_d^{(P)}$ of the P_1 maxima in Fig. 4(b). Finally, for large τ_d, all trajectories with $T_r^{(n)} \simeq \tau_d \pm T_e(\tau_d)/4$ do contribute to the primary $N_r^{(n)}$ peaks in Fig. 3(b), so that for $n=1$, $P_1(\tau_d^{(P)}) \simeq \frac{1}{2}T_e(\tau_d^{(P)})N_r^{(1)}(\tau_d^{(P)})$. The details of this quantitative analysis will be reported elsewhere; what matters here is that a substantial fraction of the renewal cycles, over 15% in Fig. 4(b), gets indeed synchronized by noise recycling.

IV. CONCLUDING REMARKS

In conclusion, we have proved that noise recycling influences the activation process in a bistable system by locking renewal trajectories at all orders. The ensuing mechanism of resonant stochastic synchronization is reminiscent of stochastic resonance [15,20], with the recycle delay time replacing the external drive period.

Extended apparatuses, like the VIRGO gravitational wave detector, working at their sensitivity threshold, can become extremely sensitive to synchronization effects. For instance, numerical simulation shows that the recycling of an additive noise induces regular oscillations in the power spectral density (PSD) of the output signal $x(t)$, no matter what its dynamics.

An example of PSD (defined as the Fourier transform of the stationary ACF) for the process (1) and (2), is displayed in Fig. 5. For correlation times of the order of the delay τ_d, the stationary ACF $\langle x(t)x(0)\rangle$ develops a bump (see inset), which corresponds to an oscillatory behavior of the PSD Such a behavior has already been observed for an overdamped oscillator driven by recycled noise [13]; therefore, to get rid of the details of the intrawell dynamics, we fed $x(t)$ through a two-state filter with thresholds $\pm x_{th}$. After filtering, damped spectral oscillations spaced by τ_d^{-1} are still observable, thus proving that τ_d actually modulates the frequency of the escape events. For the typical VIRGO feedback control times [3], spurious spikes in the output PSD are to be expected. To avoid false detection signals at the antenna operating frequencies, a revision of the filtering procedures might be needed.

[1] H. Risken, *The Fokker-Planck Equation* (Springer, Berlin, 1984).

[2] A. Papoulis, *Probability Random Variables, and Stochastic Processes* (McGraw-Hill, New York, 1991).

[3] B. Caron *et al.*, Class. Quantum Grav. **14**, 1461 (1997).

[4] G. Grüner and A. Zettl, Phys. Rep. **119**, 117 (1985).

[5] A. V. Granato and K. Lücke, in *Physical Acoustics*, edited by W. P. Mason (Academic, New York, 1966), Vol. IVA, p. 225; J. P. Hirth and J. Lothe, *Theory of Dislocations* (Wiley, New York, 1982).

[6] B. Alberts *et al.*, *Molecular Biology of the Cell* (Garland, New York, 1994).

[7] S. Matthias and F. Muller, Nature (London) **424**, 53 (2003).

[8] A. Tonomura, Rev. Mod. Phys. **59**, 639 (1987); J. F. Wambaugh, C. Reichhardt, C. J. Olson, F. Marchesoni, and F. Nori, Phys. Rev. Lett. **83**, 5106 (1999); S. Savelev, V. Misko, F. Marchesoni, and F. Nori, Phys. Rev. B **71**, 214303 (2005).

[9] Q. H. Wei, C. Bechinger, and P. Leiderer, Science **287**, 625 (2000); C. Lutz, M. Kollmann, and C. Bechinger, Phys. Rev. Lett. **93**, 026001 (2004).

[10] F. Marchesoni, Phys. Lett. A **119**, 221 (1986); S. Savelev, F. Marchesoni, P. Hanggi, and F. Nori, Europhys. Lett. **67**, 179 (2004); Phys. Rev. E **70**, 066109 (2004).

[11] Yu. S. Kivshar and A. Sànchez, Phys. Rev. Lett. **77**, 582 (1996).

[12] S. Savel'ev, F. Marchesoni, and F. Nori, Phys. Rev. Lett. **91**, 010601 (2003); **92**, 160602 (2004); B. Y. Zhu, F. Marchesoni, and F. Nori, *ibid.* **92**, 180602 (2004).

[13] M. Borromeo, S. Giusepponi, and F. Marchesoni, Phys. Rev. E **74**, 031121 (2006).

[14] M. Borromeo and F. Marchesoni, Europhys. Lett. **68**, 783 (2004); Phys. Rev. E **71**, 031105 (2005); Europhys. Lett. **72**, 362 (2005).

[15] L. Gammaitoni P. Hänggi, P. Jung, and F. Marchesoni, Rev. Mod. Phys. **70**, 223 (1998).

[16] L. S. Tsimring and A. Pikovsky, Phys. Rev. Lett. **87**, 250602 (2001); C. Masoller, *ibid.* **88**, 034102 (2002); **90**, 020601 (2003).

[17] D. Goulding *et al.* (unpublished).

[18] P. Hänggi, P. Talkner, and M. Borkovec, Rev. Mod. Phys. **62**, 251 (1990).

[19] C. R. Doering and J. C. Gadoua, Phys. Rev. Lett. **69**, 2318 (1992); M. Marchi, F. Marchesoni, L. Gammaitoni, E. Menichella-Saetta, and S. Santucci, Phys. Rev. E **54**, 3479 (1996).

[20] C. Presilla, F. Marchesoni, and L. Gammaitoni, Phys. Rev. A **40**, 2105 (1989); L. Gammaitoni, E. Menichella-Saetta, S. Santucci, F. Marchesoni, and C. Presilla, *ibid.* **40**, 2114 (1989); L. Gammaitoni, F. Marchesoni, and S. Santucci, Phys. Rev. Lett. **74**, 1052 (1995).

[21] R. Cox, *Renewal Theory* (Methuen, London, 1962).